Local-barrier-height images of TiO_2(110) surfaces

D. Ostermann,[1] G. Walther,[1] and K. D. Schierbaum[1,*]
[1]*Institut für Physik der kondensierten Materie, Abteilung Materialwissenschaft, Heinrich-Heine-Universität Düsseldorf, Universitätsstrasse 1, Gebäude 25.23, 40225 Düsseldorf, Germany*
(Received 29 October 2004; revised manuscript received 11 January 2005; published 27 June 2005)

Local barrier height (LBH) and constant current mode (CCM) images of nonreconstructed (110) single-crystalline titanium dioxide surfaces are determined under ultrahigh vacuum conditions. The barrier height measurements are performed with the tip-oscillation technique in the constant current mode (CCM) of a beetle-type scanning tunneling microscope with tunneling currents between 1 and 0.1 nA. The mean apparent height ϕ of the surface is derived as a function of the tunneling gap width. The data ϕ are in accordance with the results from $I-z$ spectroscopy. A simple electrostatic space-charge layer model explains the observed decrease of the apparent height for small tunneling gaps. The LBH technique is applied to investigate the structures of point defects on TiO_2(110) and their effects on the work function on an atomic scale. We find small concentrations of vacancies of the protruding bridging oxygen atoms, giving rise to bright atomic-scale spots between the Ti rows. The barrier height images indicate a localized and reduced apparent barrier height ϕ at these sites, in correspondence to the overall decrease in the work function Φ that has been observed earlier in ultraviolet photoelectron spectra of ion-sputtered and reduced TiO_2(110) surfaces. Besides the oxygen vacancies, the surface reveals the presence of distinct other types of atomic-scale features, both in topographic and barrier height images. Along the Ti rows, depressions with a concentration of approximately 0.02 monolayers can be identified in the constant current as well as in the barrier height images extending over one and (to a significantly lower extent) two atomic distances along [001]. They are attributed to the so-called type-B defects and they exhibit a local increase of the work function Φ.

DOI: 10.1103/PhysRevB.71.235416 PACS number(s): 68.37.Ef, 68.47.Gh

I. INTRODUCTION

Atomic-scale studies of surface defects of TiO_2(110) single crystals and the local variations of the electronic structure and work function, which are connected with the surface lattice disorder, are of great interest to an understanding of chemisorption and interface formation with metal overlayers. It is well known from a variety of experimental investigations that oxygen vacancies are formed preferentially at the (110) surface in ultrahigh vacuum due to the entropy-driven loss of lattice oxygen, thereby producing electronic donor states.[1] Many studies on chemisorption show that these sites are involved in elementary steps of the solid-gas interaction. An example is the chemisorption of TiO_2(110) with water molecules which takes place at oxygen vacancy sites of the surface.[2,3] In addition to these point defects, which are expected at $T>0$ K for thermodynamic reasons, other types of surface lattice disorder including step edges, extended defects and reconstructions occur at TiO_2(110).[4–6] They have been identified primarily by means of atomically resolved scanning tunneling microscopy (STM). This technique, in particular, has entailed considerable progress in the development of widely accepted structural models.

Until now, only a few atomic-scale investigations have been reported in which tunneling spectroscopy and apparent height measurements complement STM data of TiO_2(110) surfaces. Such techniques can resolve the local variations of the electronic structure and work functions that are induced by defects. The work function is a fundamental property of a surface and its overall sensitivity towards adsorption and defect formation is well known. A recent tunneling spectroscopy study (STS) on defective TiO_2(110) has shown an increased differential conductance at approximately -1 V which has been associated with the defect band of such surfaces which lies ~ 1 eV below the Fermi energy.[7] In this case, 1×2 reconstructed strands and step edges along [001] is the predominant type of surface disorder. Moreover, charged subsurface impurities have been found that are associated with characteristic band bending effects that affect both STM images and STS data. Maeda *et al.* have reported a local barrier height (LBH) study, carried out with the distance-oscillation technique on the clean TiO_2(110) 1×1 and the 1×2 reconstructed surface and the effect of the deposition of Au nanoparticles.[8]

Although the technique of local barrier imaging has been reported for a few metal and semiconductor surfaces[9–11] since the pioneering work by Binning, Rohrer and co-workers,[12] the interpretation of the data is not at all straightforward because of the appearance of tip-sample interaction at low tunneling widths.[13,14] This technique has not yet attained importance like STM. The sensitivity of the tunneling current I to variations of the tunneling gap z defines the apparent barrier height

$$\phi = \frac{\hbar^2}{8m}\left(\frac{d\ln I}{dz}\right)^2. \tag{1}$$

In the simplest quantum mechanic treatment of electron tunneling through a rectangular potential barrier between the tip and the sample, ϕ represents the mean work function $\frac{1}{2}(\Phi_{\text{tip}}+\Phi_{\text{sample}})$ (for small tunneling voltages $V\ll\phi$) and is related with the inverse decay length

$$\kappa = \frac{\sqrt{2m\phi}}{\hbar} \tag{2}$$

of the electron wave function outside the solid. According to Yoon *et al.*, the atomic resolution of LBH images may be explained in the idealized Tersoff-Hamann picture if one relates the current modulation to the z variation of the local density of states ρ at the Fermi level E_F, evaluated at the center of the curvature r_t of the tip,[15]

$$\frac{\partial I}{\partial z} \propto \frac{\partial}{\partial z}\left[\sum_{\nu} |\psi_\nu(r_t)|^2 \delta(E_\nu - E_F)\right] = \frac{\partial}{\partial z}\rho(r_t, E_F); \tag{3}$$

ψ_ν denotes a wave function of the sample unperturbed by the tip. The LBH images would then map the lateral variation of the tunneling current due to the decay lengths of the various surface wave functions of the sample which depend on the location in the surface Brillouin zone.[16]

A second effect, responsible for the contrast in LBH images, is the gap-width dependence of the apparent height. Theory predicts that the actual barrier drops down with decreasing gap distance due to image force and exchange-correlation effects.[17,18] The effect of barrier lowering was first shown experimentally by Binnig *et al.*, but other studies indicate contradictory results. Recently, Olesen *et al.* have presented a comprehensive experimental study for Au, Ni, and Pt single crystal surfaces in which they showed that ϕ is constant until point contact is reached if one takes into account the finite input impedance of the current preamplifier and evaluates ϕ from measurements of both the tunneling voltage and current.[19] The distance dependence of ϕ is connected with the presence of strong adhesive forces at small gap widths which lead to significant displacements of tip and sample atoms and decrease the actual tunneling width. Chen showed in a study on clean Si(111) 7×7 with a clean W tip that the experimental $\phi-z$ dependence can be fully understood by taking into account the effect of attractive and repulsive forces which follow a Morse curve and which modifies the actual displacement of the tunneling gap below approximately 3 Å.[20] In the context of the present work, we will show that the $\phi-z$ dependence is the major contrast mechanism in local-barrier images of "geometrically" ideal TiO_2(110) surfaces, that are obtained in the constant current mode. Hence, the $\phi-z$ dependence must be determined to achieve a quantitative evaluation of the LBH data of this surface.

In this report, we use weakly reduced TiO_2(110) single crystals which exhibit a small concentration of intrinsic defects. Typical bulk donor concentrations of the samples are around 10^{19} cm^3, as determined from electrical conductivities.

In the first part we describe the variation of LBH data as a function of the tunneling current. The data are used to derive the mean apparent height of the surface as a function of the tunneling gap width. This is compared with $I-z$ spectroscopy. In the second section, we will present a simple electrostatic space-charge layer model, applicable to TiO_2, which explains the observed decrease of the apparent height for small tunneling gaps. The third part of this report explores the applicability of this method to investigate the structures of point defects on TiO_2(110) and their effects on the work function on an atomic scale.

II. INSTRUMENTATION AND SAMPLE PREPARATION

The experiments were carried out in an ultrahigh vacuum system which consists of a preparation and an STM chamber. It is equipped with a homemade beetle-type scanning tunneling microscope, operated with a commercial scan unit (RHK, SPM 100). We used electrochemically etched W tips. Tunneling voltages are given with respect to the tip. The TiO_2(110) single crystals were prepared by several Ar^+ sputtering and annealing cycles at 1000 K. The electrical resistance ($R=14.8\ \Omega$) was determined in a four point arrangement with stainless steel contacts that can be pressed *in situ* to the sample's sides. We used a constant current source (Burster, Digistant 4405) and a voltage meter (Prema, 5017). The bulk conductivity is $\sigma=0.15\ \Omega^{-1}\,\mathrm{cm}^{-1}$ at room temperature, as calculated with the van der Pauw equation. Here we assume flat-band conditions without significant surface conductance. From this value we determine the bulk density of electrons, $n_b=1.5\times10^{18}$ cm^{-3}, according to $n_b=\sigma/(e\mu)$. We assume that $\mu=10^{-6}(T/K)^{-2.5}\ \mathrm{cm}^2(\mathrm{V\ s})^{-1}$ holds at a temperature of $T=300$ K.[21]

III. EXPERIMENTAL RESULTS AND DISCUSSION

A. Evaluation of LBH images and point spectroscopy

In a first set of experiments, we have determined 400×400 Å^2 wide CCM and LBH images of the clean TiO_2(110) surface at different tunneling currents I between 0.1 and 0.8 nA and a constant bias voltage of $V=1.4$ V. The resolution of the images is 512×512 pixels and the scan velocity is 100 ms per line. The root-mean-square amplitude and the frequency of the tip modulation are $\delta z=0.238$ Å and $\nu=7\times10^3$ s^{-1}, respectively. The current is step-wisely changed six times per image (with the sequence $0.1\rightarrow0.25\rightarrow0.4\rightarrow0.6\rightarrow0.8\rightarrow0.1$ nA) while both CCM and LBH data are recorded simultaneously.[26] In addition, the tunneling current is recorded. (See Fig. 1.)

Thus, the LBH image consists of six regimes from which we then determine the spatially averaged lock-in voltage. The latter is transformed into the root-mean-square amplitude of the harmonic component of I, denoted as i_{rms}. It is related to the peak value by $\hat{i}=\sqrt{2}i_{rms}$. Similarly, we obtain the corresponding tunneling current I from the current image. These values are used to determine the apparent barrier heights as described in the following.

For an oscillating tip, we assume the applicability of the relationship (1) and write for the time-dependent tunneling current,

$$I(t) = VB\exp[-A\sqrt{\phi}z(t)], \tag{4}$$

with V as voltage and B as a coefficient. The latter is proportional to the local density of states at the Fermi energy E_F and hence may show pronounced differences at the Ti and O sites of the TiO_2 surface. The value of A becomes 1.025 if ϕ

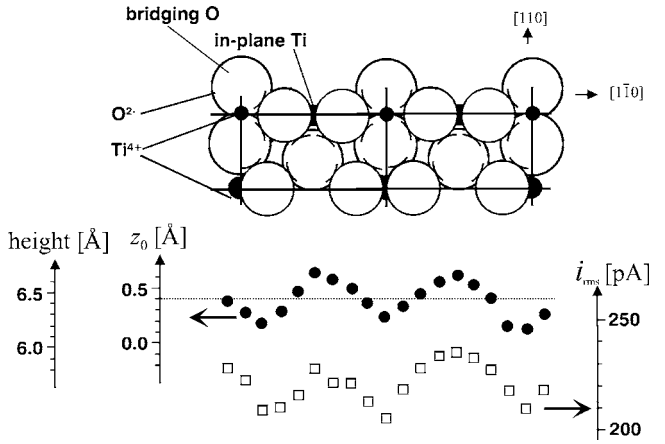

FIG. 1. Experimental values of the topographic data (i.e., height) at a tunneling current of I=0.6 nA from the CCM image of the TiO_2(110) sample 1 (solid circles) and corresponding values of the root-mean-square amplitude of the first harmonic component of the tunneling current i_{rms} (open squares) in the LBH image along [1$\bar{1}$0]. The second scale on the left hand side corresponds to the z_0 scale which is used throughout this paper. Top: Schematic cross section of the TiO_2(110) surface indicating the bridging and in-plane O atoms and the Ti atoms in fivefold (in-plane) and sixfold coordination. Further explanations are given in the text.

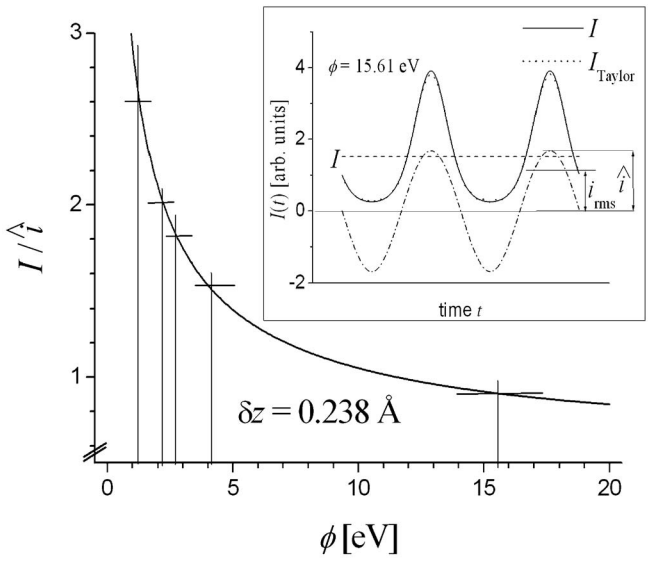

FIG. 2. Ratio $I/\hat{i}$ as a function of barrier height ϕ for δz =0.238 Å. Vertical lines correspond to experimental values of $(I/\langle\hat{i}\rangle)_{la}$. The inset shows $I(t)$, its Talyor series expansion I_{Taylor}, the time average I, the peak value $\hat{i}$, and the root-mean-square value i_{rms} for ϕ=15.61 eV.

and z are given in the units electron volt and Ångstrom. The function $z(t)$ is given by

$$z(t) = z_0 + \sqrt{2}\delta z \sin \omega t, \tag{5}$$

in which z_0 is the static displacement of the tip, δz the root mean square amplitude and $\omega = 2\pi\nu$ the angular frequency. Hence, one can write

$$I(t) = VB \exp[-A\sqrt{\phi}z_0]\exp[-A\sqrt{\phi}\sqrt{2}\delta z \sin \omega t]. \tag{6}$$

We assume that ϕ is constant during the tip oscillation. As it is shown in the Appendix A, the evaluation of this equation yields the ratio of the the time-averaged value I and the amplitude of the first harmonic component $\hat{i}$,

$$\frac{I}{\hat{i}} = \frac{1 + \frac{1}{4}b^2 + \frac{1}{64}b^4}{b + \frac{1}{8}b^3}, \tag{7}$$

with $b = -A\sqrt{\phi}\sqrt{2}\delta z$.

Figure 2 displays the calculated ratio $I/\hat{i}$ as a function of ϕ. An approximate solution of the polynomial (7) is

$$\sqrt{\phi} = \frac{2}{A\delta z}\left[\frac{I}{i_{rms}} - \sqrt{\left(\frac{I}{i_{rms}}\right)^2 - 1}\right], \tag{8}$$

if one neglects the third- and fourth-order term. Note that b refers to a situation in which ϕ does not alter during the tip oscillation, i.e., the amplitudes are sufficiently small. In most cases, large amplitudes are necessary to reduce the noise-to-signal ratio or to obtain spatially resolved information. This gives rise to a *systematic* error in the determination of $I/\hat{i}$ and hence of ϕ if its value depends on the gap width.

We will assign the experimental $I/\hat{i}$ data with the index "la" that signifies that large amplitudes have been applied. Corresponding barrier heights deviate therefore from the actual values and are denoted with ϕ_{la}. We will demonstrate in the following that one can take ϕ_{la} as the first estimated values to obtain more accurate data of ϕ. By using the function $I/\hat{i}(z_0)$, we determine the barrier heights from the ratio of the spatially averaged values of $\langle\hat{i}\rangle = \sqrt{2}\langle i_{rms}\rangle$. The results are given in Table I. The value of $\langle\phi\rangle_{la}$ refers to the mean value of the surface. It can be concluded from the decreasing slope of the function $I/\hat{i}(z_0)$ (compare with Fig. 2) that the statistical error of $\langle\phi\rangle_{la}$ becomes larger at lower tunneling currents if one assumes a constant absolute uncertainty in the determination of I and $\langle\hat{i}\rangle$. The statistical errors in $\langle\phi\rangle_{la}$ have been computed for the lowest and highest values from the standard deviations in the images of the currents I and $\hat{i}$.

TABLE I. Spatially averaged values of the root-mean-square amplitudes $\langle i_{rms}\rangle$ at different tunneling currents I. Barrier heights $\langle\phi\rangle_{la}$ are determined from the plot $I/\hat{i}$ vs ϕ in Fig. 2. The values of $\langle\phi\rangle$ are determined from Eq. (11).

I/nA	$\langle i_{rms}\rangle$/nA	$\left(\frac{I}{\langle\hat{i}\rangle}\right)_{la}$	$\langle\phi\rangle_{la}$/eV	$\langle\phi\rangle$/eV
0.118±0.005	0.0923±0.005	0.90±0.09	15.61±4	5.48±0.7
0.255	0.1180	1.53	4.04	3.10
0.411	0.1594	1.82	2.74	2.33
0.603	0.2186	1.95	2.37	1.91
0.812±0.005	0.2216±0.005	2.59±0.09	1.30±0.08	1.60±0.1

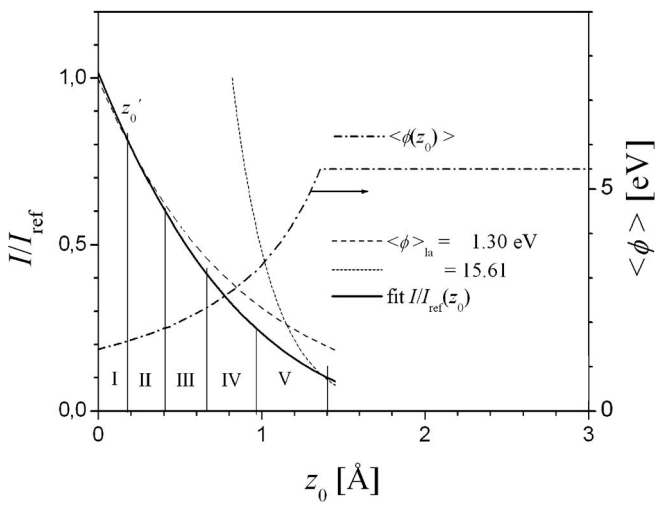

FIG. 3. Relative tunneling current I/I_{ref} (solid line) and barrier height $\langle\phi\rangle$ (dot-dashed line) as a function of distance z_0. The value z_0=1.4 Å corresponds to the lowest tunneling current. Further explanations are given in the text.

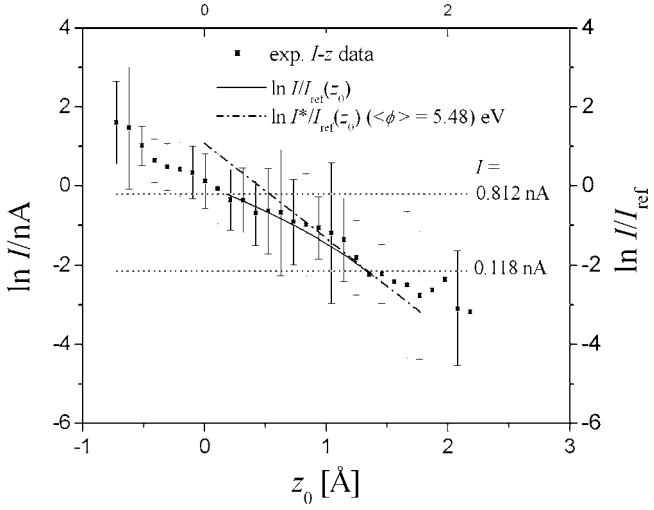

FIG. 4. Experimental ln $I-z$ data from point spectroscopy (dots) and calculated ln(I/I_{ref}) values (solid curve) as a function of z_0. The dot-dashed line corresponds to a hypothetical z_0 dependence of the current ln(I^*/I_{ref}) if one assumes a constant apparent height of $\langle\phi\rangle$=5.48 eV. The z_0 data are referenced to z_0 at which I is 1 nA. The dotted lines indicate the low and high tunneling currents in the tip-oscillation measurements of $\langle\phi\rangle$.

The next step in the refinement of our determination of $\langle\phi\rangle$ concerns the calculation of the current-distance curves. We use the relationship

$$I = I_{ref} \exp[-A\sqrt{\langle\phi\rangle_{la}} z_0]. \quad (9)$$

Here, we refer I to a value of I_{ref}=1 nA that we attribute to z_0=0 (at a certain gap width or topographic height, see Fig. 1).

The iteration is based on a fitting procedure in which five individual functions $I/I_{ref}(z_0)$ are calculated that reflect the behavior of I in the intervals I to V (Fig. 3). The procedure is explained in Appendix B. The first function $I/I_{ref}(z_0)$ at $\langle\phi\rangle_{la}$=1.30 eV holds between 1 nA and 0.603 nA (dashed line, used as the start function of the iteration). The dotted curve depicts the function $I/I_{ref}(z_0)$ and corresponds to the last step of the iteration at $\langle\phi\rangle_{la}$=15.61 eV. The other curves are not shown in Fig. 3 for a simplification.

In order to obtain a common I/I_{ref} curve for the entire experimentally adjusted range of z_0, we then calculate a fourth-order polynomial function I/I_{ref} that fits the individual I/I_{ref} curves in the different regimes (solid line labeled "fit"),

$$I/I_{ref} = 1.017 - 1.220z_0 + 0.530z_0^2 - 0.1z_0^3 + 0.007z_0^4. \quad (10)$$

z_0 is given in the unit Ångstrom. From this function, one obtains the mean apparent barrier height of the TiO_2(110) surface from

$$\langle\phi\rangle = 1.025\left[\frac{d\ln(I/I_{ref})}{dz_0}\right]^2. \quad (11)$$

The numeric determination yields the $\langle\phi\rangle$-z_0 relationship which is revealed by the dot-dashed curve in Fig. 3. As the minimum experimental value of I is 0.118 nA, an upper limit of the determination of $\langle\phi\rangle$ appears, being 5.48 eV. A physically more realistic model would give a progressive transition from the polynomial (10) into this limit which has not been considered in Fig. 3. The values $\langle\phi\rangle$ are given in Table I for the experimentally chosen tunneling currents. We estimate the error in $\langle\phi\rangle$ in such a way that we repeat the fitting procedure described above and take into account the variation of $\langle\phi\rangle_{la}$.

One expects barrier heights close to $\langle\phi\rangle=(\Phi_W+\Phi_{TiO_2}-eV)/2\approx(4.55+5.2-1.4)/2=4.2$ eV for low tunneling currents and hence larger tip-sample spacing. In the next part of this report we will show that one must take into account that a significant portion of the applied bias voltage of 1.4 V drops down within a space-charge region of TiO_2. Hence, eV is smaller (0.18 eV) and one obtains $\langle\phi\rangle$=4.8 eV which is closer to our low-current value of $\langle\phi\rangle$ and in the range of the estimated error. Moreover, one may also attribute the difference between these values to a higher work function of the W tip at the apex. Maeda *et al.* have reported a local work function of 4.95 eV of the "ideal" surface from their LBH data.[8] They employed very large tip oscillation amplitudes of 2.5 to 5 Å and did not comment on the gap-width dependence of ϕ.

It is evident that the large barrier heights $\langle\phi\rangle_{la}$ at low tunneling currents differ from the more consistent values of $\langle\phi\rangle$. The difference leads to the significant deviation between the fitted overall $I/I_{ref}(z_0)$-function and the $I/I_{ref}(z_0)$ curve for $\langle\phi\rangle_{la}$=15.61 eV in Fig 3. A detailed analysis of this problem is given in Appendix C.

We have also determined conventional $I-z$ curves ("point spectroscopy"). Figure 4 shows a typical result for a clean TiO_2(110) surface, together with the overall ln $I/I_{ref}(z_0)$-function of Fig. 3 (solid line).

Here, the z scale has been adapted to the z_0 scale. The standard deviation of I has been computed from ten $I-z$

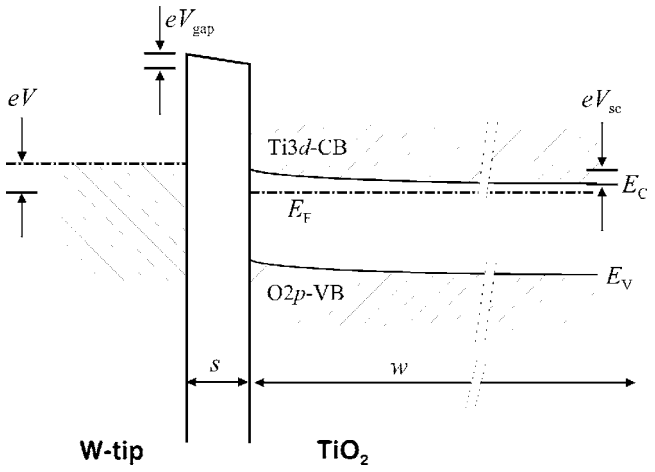

FIG. 5. Energy band diagram of the system W/TiO_2 separated by a narrow vacuum gap of the width s under an applied external bias voltage V. Potentials at the gap and the TiO_2 depletion layer are V_{gap} and V_{sc}, respectively. The donor states which are associated with the oxygen vacancies in the TiO_2 are not shown. For a description, see the text.

curves. We find a good agreement of the point spectroscopy data with the fitted curve. It is evident that point spectroscopy exhibits a large statistical error when compared with the tip-oscillation technique. We have also computed the values of $\ln I/I_{ref}$ for 0 Å $\leqslant z_0 \leqslant$ 1.4 Å for the case that the apparent height $\langle\phi\rangle$=5.48 eV (which corresponds to the tunneling current of 0.118 nA) is constant upon variation of the gap width. The result is depicted by the dot-dashed line and shows a significant deviation from the point spectroscopy data at lower values of z_0. By comparison we find that the $I-z$ data reveal a decreasing slope with a decreasing gap width. Moreover, the $I-z$ data give evidence of an upper limit of the apparent height as we have assumed in Fig. 3. We will now deal with the effect of the gap width on the apparent height in more detail. It was previously pointed out by Bonnell that tips and voltage induced band bending effects occur in STM experiments on transition metal oxide surfaces.[22]

B. Gap-width dependence of the apparent height

Figure 5 depicts a schematic energy band diagram of the tunneling gap and the important energy levels associated with the W tip and the TiO_2. We assume the work function of the W tip is equal to Φ_W=4.55 eV. From ultraviolet photoelectron spectra, Φ_{TiO_2}=5.2 eV has been determined for the clean and geometrically ideal TiO_2 surface.[23] We determine the bulk position of the Fermi energy E_F relative to the conduction band minimum E_C in the Boltzmann approximation,

$$E_C - E_F = kT \ln \frac{n_b}{N_C} = -0.2 \text{ eV}, \tag{12}$$

where N_C denotes the effective density of states, calculated with an effective electron mass of $20m_e$ for a temperature of T=300 K. Hence, the electron affinity χ_{TiO_2} of TiO_2 is 5.0 eV. Furthermore, we assume that the surface density of electronic states in the band gap of TiO_2(110) is negligible so that the conduction and valence bands are not pinned with respect to E_F. These band gap states are associated with intrinsic defects whereas the Ti and O-derived "dangling bonds" of the undercoordinated ions at the surface are energetically localized in the region of the conduction and valence bands and are therefore completely empty or occupied. The depicted situation bears analogy with an ideal metal-oxide-semiconductor capacitor. In this case, the band bending at the semiconductor is determined by the difference in the work functions at zero applied bias voltage. The band bending can be removed and flat band condition is reached by applying a compensating external bias given by

$$V_{fb} = \Phi_M - \chi_S - E_C + E_F = \Phi_M - \Phi_S, \tag{13}$$

where Φ_M and Φ_S are the metal and semiconductor work functions and χ_S is the semiconductor electron affinity. On the other hand, an ideal Schottky barrier may be formed if the vacuum gap separating tip and sample finally disappears upon reducing the gap width. Then the Schottky-Mott rule,

$$\phi_{SB} = \Phi_M - \chi_S, \tag{14}$$

holds.

Here ϕ_{SB} denotes the barrier height. It is obvious that the difference V between the electrostatic potentials outside the surfaces of the metal and the semiconductor tend to zero upon reducing the gap width and disappears altogether when an intimate contact is formed. In order to evaluate quantitatively the effect of variations of the vacuum-gap width s, one may treat the system as to consist of two capacitors that are connected in series. For the gap we write

$$C_{gap} \propto s^{-1} \tag{15}$$

as capacitance per unit area, and for the depleted region in the TiO_2,

$$C_{sc} \propto \varepsilon w^{-1}, \tag{16}$$

as the differential capacitance. Here, w denotes the width of the space charge layer. Its value can be calculated in the depletion approximation,[24]

$$w = l_D \sqrt{\frac{2eV_{sc}}{kT}}. \tag{17}$$

Here,

$$l_D = \sqrt{\frac{\varepsilon\varepsilon_0 kT}{e^2 N_D}} \tag{18}$$

is the Debye length for a semiconductor with fully ionized donors. For TiO_2 with a dielectric coefficient ε of approximately 100, we calculate l_D=139 Å and 438 Å $\leqslant w \leqslant$ 1028 Å for 0.1 Å $\leqslant s \leqslant$ 10 Å at T=300 K. We have assumed $n_D = 0.5n_b$, i.e., doubly ionized donor states, for the sake of simplicity. Even for typical tunneling gaps, the value of the differential capacitance becomes comparable with C_{gap} due to the large value of the dielectric coefficient of TiO_2.

The voltage applied between the tungsten tip and the TiO_2 drops down over the tunneling gap and the depletion region.

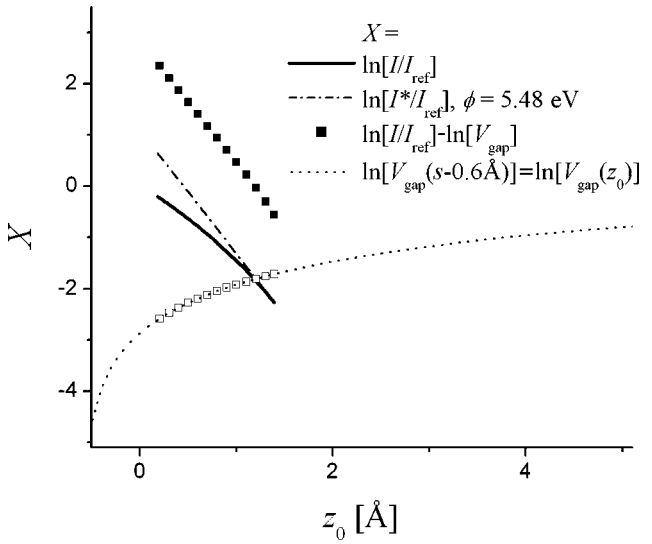

FIG. 6. Tunneling current I/I_{ref} (thick solid line) and gap voltage V_{gap} (in volts) as a function of the gap width z_0 (dotted line). Further explanations are given in the text.

Only for larger distances, $V_{\mathrm{gap}}=V$ holds. One can determine the voltage drop in the TiO_2 from the total capacitance,

$$\frac{1}{C}=\frac{1}{C_{\mathrm{gap}}}+\frac{1}{C_{\mathrm{sc}}} \tag{19}$$

and

$$V_{\mathrm{sc}}=V\frac{C_{\mathrm{gap}}/C_{\mathrm{sc}}}{1+C_{\mathrm{gap}}/C_{\mathrm{sc}}}. \tag{20}$$

Correspondingly, the gap potential is

$$V_{\mathrm{gap}}=V-V_{\mathrm{sc}}, \tag{21}$$

which yields $0.0097\ \mathrm{V}\leqslant V_{\mathrm{gap}}\leqslant 0.69\ \mathrm{V}$ for an applied bias voltage of 1.4 V ($0.1\leqslant s\leqslant 10$ Å). Evidently, the voltage drop over the tunneling gap is not at all constant when the tip-sample distance is changed. As shown in Fig. 6, the difference $\ln(I/I_{\mathrm{ref}})-\ln(I^*/I_{\mathrm{ref}})$ becomes larger when z_0 decreases. This behavior is consistent with a corresponding decrease of the gap voltage. We will now investigate whether this effect is related to the observed current-distance behavior and the decrease of the apparent height. We have included the $\ln(I/I_{\mathrm{ref}})$ vs z_0 graph in the same diagram, together with the straight line $\ln(I^*/I_{\mathrm{ref}})$ vs z_0 at a constant apparent height of $\langle\phi\rangle=5.48$ eV. For a quantitative comparison, one must align the scales s and z_0 (Fig. 6). The criterion for the alignment is whether the difference $\ln(I/I_{\mathrm{ref}})-\ln(V_{\mathrm{gap}})$ vs z_0 (which is associated with the tunneling conductance g) exhibits the same slope than the "ideal" $\ln(I^*/I_{\mathrm{ref}})$ vs z_0 curve (V_{gap} is given in volts). In this case, $\ln(I/I_{\mathrm{ref}})$ vs $\ln(V_{\mathrm{gap}})$ follows a function of the type $g\propto\exp(-1.025\sqrt{\langle\phi\rangle}z_0)$ with a constant value of ϕ.

Figure 6 shows that such a situation occurs if the $\ln(V_{\mathrm{gap}})$ curve is shifted by −0.6 Å with respect to the z_0 scale (dotted line). Here, the $\ln(V_{\mathrm{gap}})$ values which are marked as open squares have been used to calculate the difference $\ln(I/I_{\mathrm{ref}})-\ln(V_{\mathrm{gap}})$ (solid squares). We conclude that the tunneling conductance would indicate a *constant* apparent height over the entire range of widths from 0.18 to 1.4 Å if the bias voltage is V_{gap} instead of V. Similar to the interpretation given by Olesen *et al.*, our findings suggest that the *tunneling voltage depends on the gap width*. This dependence leads to the reduction of $\langle\phi\rangle$. In contrast to their work, however, we cannot measure the gap voltage since the bias voltage drops down within the TiO_2 crystal. In spite of simplified treatment of the tip's geometry, our electrostatic space charge model explains the observed decrease of the apparent height quantitatively. We will now analyze the effects of intrinsic defects on TiO_2(110) on the apparent barrier height which are observed in the LBH images.

C. Point defects

Point defects can be easily created at TiO_2(110) surfaces by heating crystals in ultrahigh vacuum to high temperatures of about 1000 K.[1] This process is usually kinetically controlled as point defects exhibit high diffusion coefficients in the bulk, thus generating nonequilibrium defect distributions. Recent STM studies have shown that oxygen vacancies V_{o} can be identified on TiO_2(110) surfaces[25] and can be distinguished from hydroxyl groups.[3] The vacancies are formed by the desorption of molecular oxygen and result from missing oxygen atoms at two-fold coordinated bridging sites. They are associated with bright spots which appear in STM images between the ⟨001⟩ rows of the fivefold-coordinated surface Ti atoms.

Figure 7(a) shows the CCM map of a (110) terrace on which such oxygen vacancies are visible among other types of pointlike features. They are marked by V_{o}. One estimates a surface concentration of approximately $5\times10^{12}\ \mathrm{cm}^{-2}$ from the image which corresponds to the model of statistically distributed and noninteracting point defects. The value is lower than the reported defect density of TiO_2(110) after a high-temperature treatment at 1100 K and a subsequent O_2 dosing of 100 L which might result from a lower heating temperature in our study. The LBH map [Fig. 7(b)] indicates a reduced value of i_{rms} at the positions of the oxygen vacancies.

Quantitative data can be derived from the line profile along line A which is depicted in Fig. 8. We determine 30 pA at V_{o} and approximately 75 pA at the regular Ti sites. These values correspond to 1.81 and 0.73 of $(I/\hat{i})_{\mathrm{la}}$, respectively, using $\hat{i}=\sqrt{2}Ji_{\mathrm{rms}}$ and $I=85$ pA. [Table I provides a relationship between the large-amplitude values of the ratio $(I/\langle\hat{i}\rangle)_{\mathrm{la}}$ and the spatially averaged apparent height $\langle\phi\rangle$ for ratios in the range between 2.59 and 0.90, which almost cover the range of $(I/\hat{i})_{\mathrm{la}}$ values in the LBH image]. The polynomial fit of the values of the Table I yields

$$\langle\phi\rangle=8.29-1.82\left(\frac{I}{\langle\hat{i}\rangle}\right)_{\mathrm{la}}-2.06\left(\frac{I}{\langle\hat{i}\rangle}\right)_{\mathrm{la}}^{2}+0.68\left(\frac{I}{\langle\hat{i}\rangle}\right)_{\mathrm{la}}^{3}. \tag{22}$$

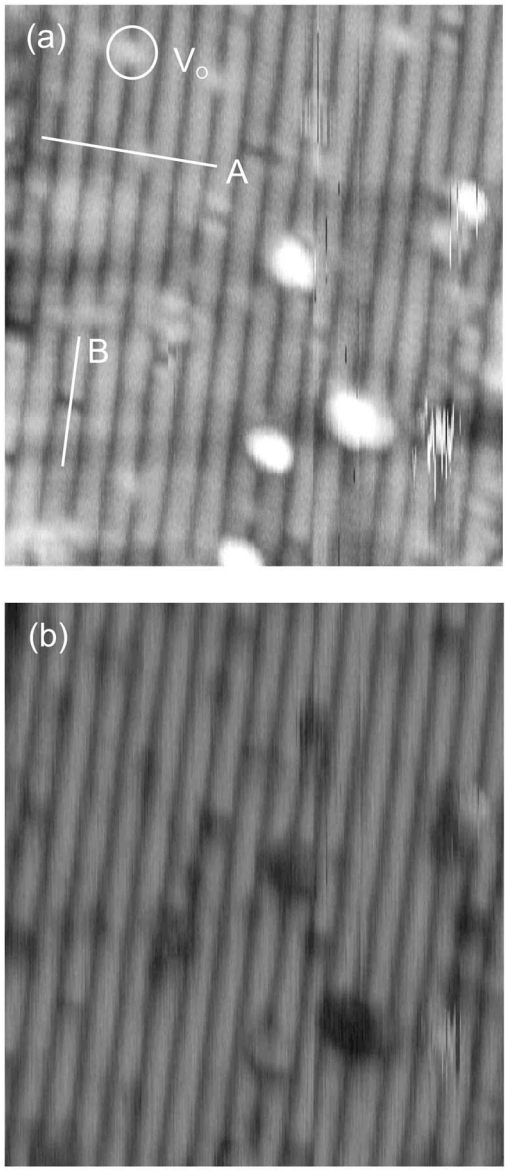

FIG. 7. (a) CCM and (b) LBH image of TiO_2(110) (sample 2). Scan range: 110×150 Å^2; bias voltage $V=1.4$ V; tunneling current $I=0.085$ nA; tip oscillation: root-mean-square amplitude $\delta z=0.238$ Å, frequency 7000 s^{-1}. Further explanations are given in the text.

This function is also applicable to calculate the spatially resolved apparent heights $\phi(x_{1\bar{1}0})$ from the data $\hat{i}(x_{1\bar{1}0})=\sqrt{2}i_{\mathrm{rms}}(x_{1\bar{1}0})$.

The result is shown in Fig. 9 by the dotted line, labeled "$\phi(x_{1\bar{1}0})$." As outlined in Appendix B, ϕ depends on the gap width which alters along the $x_{[1\bar{1}0]}$ direction due to the corrugation of ~0.5 Å. This was explained by the distance dependence of the tunneling voltage V. Consequently, the value $\phi(x_{1\bar{1}0})$ is the apparent barrier at a certain gap width or, by referring to our z_0 scale, at a certain value of z_0. In order to compensate the distance dependence, which appears in $\phi(x_{1\bar{1}0})$, one may compute the spatially averaged apparent height $\langle\phi\rangle$ of the surface at the same gap width (i.e., the same value of z_0) as the function of $x_{1\bar{1}0}$. We can apply the $\langle\phi\rangle(z_0)$ polynomial, which is given in Appendix C, to obtain the function $\langle\phi\rangle(x_{1\bar{1}0})$. To do so, one must convert the height scale of Fig. 8 into a z_0 scale by introducing a (constant) displacement Δz between both scales. The value of Δz is varied until the mean values $\overline{\langle\phi\rangle(x_{1\bar{1}0})}$ and $\overline{\phi(x_{1\bar{1}0})}$ become equal. (The averaging is performed in the region outside the vacancy.) The curve $\langle\phi\rangle(x_{1\bar{1}0})$ is depicted by the solid line in Fig. 9. The displacement is $\Delta z=-0.55$ Å and the z_0 scale agrees reasonably well with the z_0 scale of Fig. 1. It is, however, evident that the maximum values of $\langle\phi\rangle(x_{1\bar{1}0})$ are larger than 5.48 eV and beyond the range for which the applicability of the polynomial (C1) has been evidenced (compare with Fig. 3). Taking also into account the statistical errors of $\langle\phi\rangle$

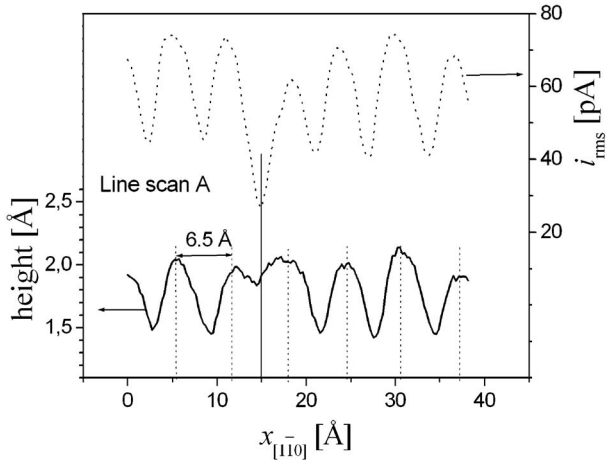

FIG. 8. Line scan along A of the CCM (solid curve) and LBH images (dotted curve) of Fig. 7. Vertical dotted lines indicate in-plane Ti sites; the solid line refers to the position of an oxygen vacancy.

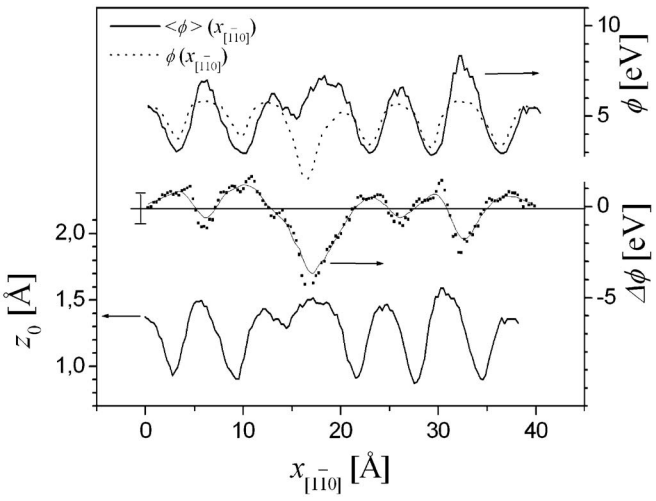

FIG. 9. Line scan of the topographic data of Fig. 7 in a plot z_0 vs $x_{1\bar{1}0}$. The apparent barrier height ϕ is obtained from the i_{rms} data (dotted curve). The apparent barrier height $\langle\phi\rangle$ as calculated from the z_0 values (solid curve). $\Delta\phi$ shows the difference between the solid and dotted curves.

that are given in Table I, one concludes that there is no significant difference between both curves at the in-plane Ti (maxima) and bridging O sites (minima) whereas the difference is significant at the vacancy site. The difference,

$$\Delta\phi = \phi(x_{1\bar{1}0}) - \langle\phi\rangle(x_{1\bar{1}0}), \tag{23}$$

is shown by the thin solid curve in Fig. 9, together with an error bar. It represents the deviation of the apparent height from the spatially averaged apparent height at an (approximately) identical gap width. Ideally, $\Delta\phi$ does not exhibit a z_0 dependence, in contrast to the $\phi(x_{1\bar{1}0})$ curve. This demonstrates that LBH images and line scans can only be evaluated by taking quantitatively into account their gap width dependence. There is one exception, of course, with respect to LBH data that are taken at different sites of the surface but at identical topographic heights which can be directly evaluated. This situation is almost fulfilled for the in-plane Ti site and the oxygen vacancy. We find a strong decrease with a negative value of $\Delta\phi \approx -3.8$ eV at the oxygen vacancy site. This may be attributed to a reduced work function Φ at the oxygen vacancy of about 1.4 eV. A local work function of 1.9 eV has been reported by Maeda *et al.* for strong reduced $TiO_2(110)$ surfaces, exhibiting a (1×2) reconstruction.[8] Such a reduction of Φ is in correspondence with the overall decrease in the work function ϕ to about 3 eV that has been observed earlier in ultraviolet photoelectron spectra of ion-sputtered and reduced $TiO_2(110)$ surfaces, although the degree of quantitative agreement remains a subject for further experimental improvements of the measurements.

The second type of pointlike defects appears on the Ti rows as depressions in the CCM image, which are labeled here as a "type-B" defect in accordance with Diebold's notation.[4] They extend over one and (to a significantly lower extent, see also Fig. 7) two atomic distances along [001]. Although the existence of these defects is well known for $TiO_2(110)$ surfaces, their nature is still under debate. Subsurface defects have been proposed which possibly could consist of missing oxygen atoms under the in-plane Ti ions, thereby producing a reconstruction with minima in the topography.

Later, Fig. 10 reveals the line scan along B in a z_0 vs $x_{[001]}$ plot that is calculated from the topographic height according to the procedure described above. We also include a 6 Å long arrow (i.e., twice the surface lattice unit in the [001] direction, 2×2.96 Å), indicating the lateral dimension of this defect. Figure 10 shows also the effect on the apparent height ϕ and on $\Delta\phi$. It is obvious that this defect is associated with a local increase of ϕ. The CCM images show that the majority of the B-type defects appear brighter on both sides that neighbor the depression in the [001] direction. On a few spots we notice point defects that appear such as they are composed of two adjacent B-type defects on neighbored Ti rows. Although the LBH variations are similar, the nature of these features remains as an open problem like the type-B defect itself. The same holds for the adsorbates at the surface, which appear in the CCM images as bright spots between the Ti rows. Interestingly, they lead to different "fingerprints" in the LBH images. The majority of them are

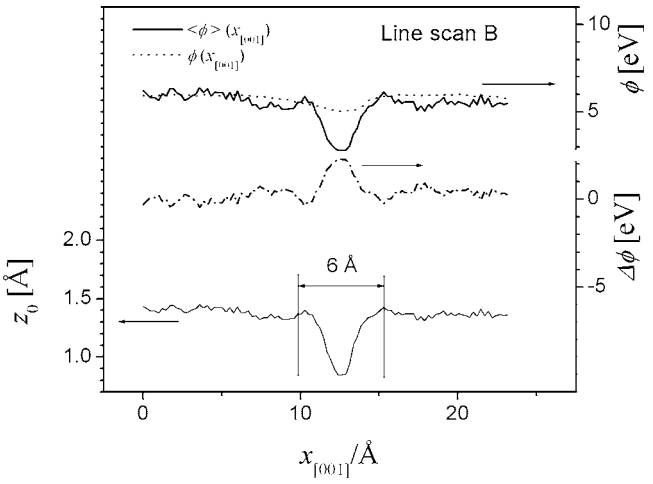

FIG. 10. Line scan along B of the CCM and LBH images of Fig. 7.

associated with depressions, but they may also appear as protrusions. The topographic heights at these spots exceed the surface plane by about 2.3 Å. This is likely related to more pronounced changes of the local density of states and beyond the applicability of our evaluation method.

IV. SUMMARY AND CONCLUSIONS

We have employed the tip-oscillation technique, complemented by conventional constant-current-mode STM, to image intrinsic defects on the $TiO_2(110)$ surface and to investigate how they influence the work function on an atomic scale. As an important step towards an accurate measurement of apparent heights and their dependence on the tunneling widths, we have demonstrated and discussed an evaluation procedure for LBH data and compared it with point spectroscopy. A simple electrostatic space charge model, based on well known semiconductor physics approaches, has been proposed and applied to TiO_2 that explains quantitatively the observed gap-width dependence of the apparent height. It is applicable to weakly reduced (110) surfaces on which the concentration of band gap states, that are attributed to Ti3*d* states and associated with oxygen vacancies, is small and hence a pinning does not occur. This model has interesting implications for scanning tunneling spectroscopy, employed to such surfaces, as this model may provide information on the actual gap voltage as a function of the bias.

In the third part we have demonstrated that this LBH method provides an access to local work function changes which are induced by surface oxygen vacancies. Other types of pointlike defects have been found, including type-B defects.

ACKNOWLEDGMENTS

This work is funded by the European Community under Project No. 505895-1. Stimulating discussions with G. Thornton (University College London) are gratefully acknowledged.

APPENDIX A: CALCULATION OF $I/\hat{i}$

If one applies a Taylor series expansion to $\exp[-A\sqrt{\phi}\sqrt{2}\delta z \sin \omega t]=\exp[b \sin \omega t]$ with $b=-A\sqrt{\phi}\sqrt{2}\delta z$ and uses the trigonometric expressions $\sin^2 \omega t=\frac{1}{2}(1-\cos 2\omega t)$, $\cos^2 \omega t=\frac{1}{2}(1+\sin 2\omega t)$, and $\sin^3 \omega t=-\frac{1}{4}(\sin 3\omega t - 3 \sin \omega t)$ one obtains for the tunneling current

$$I(t) = VB \exp[-A\sqrt{\phi}z_0]\left(1 + b \sin \omega t + \frac{1}{4}b^2 - \frac{1}{4}b^2 \cos 2\omega t - \frac{1}{24}b^3 \sin 3\omega t + \frac{1}{8}b^3 \sin \omega t + \frac{1}{64}b^4 - \frac{1}{64}b^4 \cos 2\omega t \pm \cdots\right). \quad \text{(A1)}$$

Truncation after the fourth-degree term yields the amplitude of the first harmonic component of I,

$$\hat{i} = \left| VB \exp[-A\sqrt{\phi}z_0]\left(b + \frac{1}{8}b^3\right)\right|, \quad \text{(A2)}$$

for which we take positive values only. In a similar fashion, one can write for the time-averaged value of I,

$$I(t) = VB \exp[-A\sqrt{\phi}z_0]\left(1 + \frac{1}{4}b^2 + \frac{1}{64}b^4\right). \quad \text{(A3)}$$

Note that the term $\left(1+\frac{1}{4}b^2+\frac{1}{64}b^4\right)$ is associated with an increase of the tunneling current when the tip is oscillating.[27] Equations (A2) and (A3) suggest that the term $VB \exp[\sqrt{\phi}]$ is cancelled out by division. It is trivial that this applies to $\exp(z_0)$ as LBH and CCM images are recorded simultaneously, i.e., at the same value of z_0.

It is, however, not as simple for the expression $VB \exp\sqrt{\phi}$. As shown in Fig. 1, i_{rms} and hence $\hat{i}$ vary laterally while I is constant. The variation of along $[1\bar{1}0]$ reveals the periodicity of the surface lattice unit (6.5 Å) like the topographic data. As the consequence, the ratio $I/\hat{i}$ should be determined from the $\hat{i}$ data at identical sites (e.g., at the minima or maxima). Since a sufficient atomic resolution is not obtained at all values of I, we compute the spatial average of $\langle\hat{i}\rangle$ from the LBH image. (In the following, we use $\langle\ \rangle$ when spatially averaged data must be indicated.)

The procedure of averaging $\langle\hat{i}\rangle$ is suitable since the ratio of the bridging O and in-plane Ti sites, at which the largest differences of $\langle\hat{i}\rangle$ occur, is close to 1 and the number of defects and adsorbates is small. Similarly, we determine $\langle I\rangle$ from the current image to increase the accuracy for the values of I. From the Eqs. (A1) and (A2), we then obtain the ratio

$$\frac{I}{\hat{i}} = \frac{1 + \frac{1}{4}b^2 + \frac{1}{64}b^4}{b + \frac{1}{8}b^3}. \quad \text{(A4)}$$

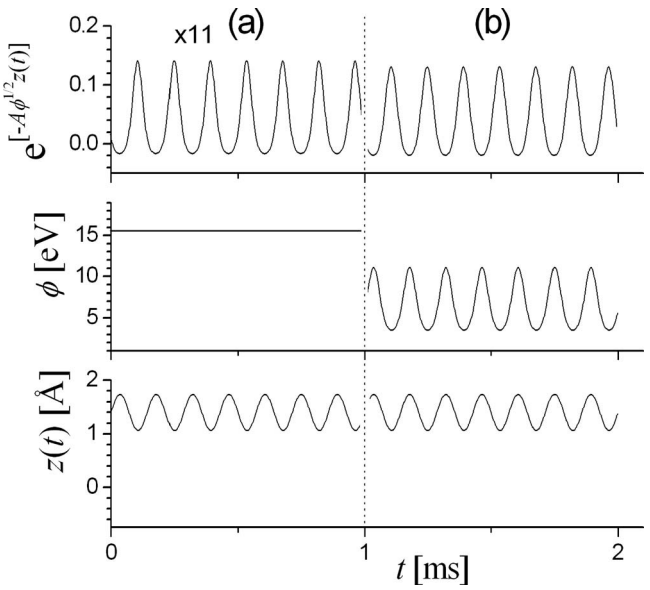

FIG. 11. $\exp[-A\sqrt{\phi}z(t)]$, $\phi(t)$ and $z(t)$ as a function of time t for an oscillating tip. Further explanations are given in the text.

APPENDIX B: DETERMINATION OF $I/I_{\mathrm{ref}}(z_0)$

We first calculate the function $I/I_{\mathrm{ref}}(z_0)$ from Eq. (9), using $\langle\phi\rangle_{\mathrm{la}}=1.30$ eV that passes through the value 0.812 in the interval I. At the low-current value of I/I_{ref} at the border between the intervals I and II (and, hence, at a certain value z_0') we calculate a new function $I/I_{\mathrm{ref}}=\exp[-A\sqrt{2.37\ \mathrm{eV}}(z_0+\Delta z)]$ in such a way that both curves have the same value of I/I_{ref} at $z_0'=z_0+\Delta z$. Graphically, Δz corresponds to a horizontal shift of the curve I/I_{ref}. If we repeat this procedure, five I/I_{ref} curves are generated which individually reflect the tunneling current-*versus*-distance relationships in a small range of z_0. These ranges correspond to the intervals I to V in Fig. 3.

APPENDIX C: EFFECT OF OSCILLATING APPARENT HEIGHT

We obtained the barrier height $\langle\phi\rangle_{\mathrm{la}}$ by evaluating I and $\langle\hat{i}\rangle$. The relationship with Eq. (4) is illustrated by Fig. 11. It indicates the oscillation of $\exp[-A\sqrt{\langle\phi\rangle}z(t)]$ (to which the tunneling current is proportional) for two different cases. The image (a) shows the situation if one assumes a constant tunneling barrier height in the evaluation of the experimental data. We choose $\langle\phi\rangle_{\mathrm{la}}=15.61$ eV and $z_0=1.4$ Å in line with the values at a tunneling current of $I=0.118$ nA.

The image (b) demonstrates the case of an oscillating tip ($\nu=7\times10^3\ \mathrm{s}^{-1}$, $\delta z=0.238$ Å, and $z(t)=z_0+\sqrt{2}\delta z \sin \omega t$ with $z_0=1.4$ Å) and an oscillating barrier height $\langle\phi\rangle(t)$. We have computed $\langle\phi\rangle(t)$ from the $\langle\phi\rangle-z_0$ curve of Fig. 1 by means of a fourth-order polynomial fit,

$$\langle\phi\rangle = 1.431 + 0.073z_0 + 3.959z_0^2 - 4.532z_0^3 + 2.346z_0^4 \quad \text{(C1)}$$

($\langle\phi\rangle$ and z_0 are given in the units eV and Ångstrom, respectively). Here, the values of $\exp[-A\sqrt{15.61\ \mathrm{eV}}z(t)]$ are multi-

plied by a factor of 11, to adjust the scales. It can be easily shown by Fourier analysis (which is not illustrated here) that the same ratios $I/\langle\hat{i}\rangle$ are obtained as in (a). This comparison demonstrates that the finite value of δz represents a major source for systematic errors in the determination of $\langle\phi\rangle$. Consequently, it appears to be necessary to determine LBH data at different tunneling currents and hence different tunneling widths for a quantitative analysis of images.

*Corresponding author. Electronic address: schierb@uni-duesseldorf.de

[1] W. Göpel, G. Rocker, and R. Feierabend, Phys. Rev. B **28**, 3427 (1983).
[2] I. M. Brookes, C. A. Muryn, and G. Thornton, Phys. Rev. Lett. **87**, 266103 (2001).
[3] R. Schaub, P. Thostrup, N. Lopez, E. Lægsgaard, I. Stensgaard, J. K. Nørksov, and F. Besenbacher, Phys. Rev. Lett. **87**, 266104 (2001).
[4] U. Diebold, Surf. Sci. Rep. **48**, 53 (2003).
[5] M. Sander and T. Engel, Surf. Sci. Lett. **302**, L263–L268 (1994).
[6] R. A. Bennett, P. Stone, N. J. Price, and M. Bowker, Phys. Rev. Lett. **82**, 3831 (1999).
[7] M. Batzill, K. Katsiev, D. J. Gaspar, and U. Diebold, Phys. Rev. B **66**, 235401 (2002).
[8] Y. Maeda, M. Okumura, S. Tsubota, M. Kohyama, and M. Haruta, Appl. Surf. Sci. **222**, 409 (2004).
[9] B. Marchon, P. Bernhardt, M. E. Bussell, G. A. Somorjai, M. Salmeron, and W. Siekhaus, Phys. Rev. Lett. **60**, 1166 (1988).
[10] R. Wiesendanger, L. Eng, H. R. Hidber, P. Oelhafen, L. Rosenthaler, U. Staufer, and H.-J. Güntherodt, Surf. Sci. **189/190**, 24 (1987).
[11] L. Olesen, M. Brandbyge, M. R. Sørensen, K. W. Jacobsen, E. Lægsgaard, I. Stensgaard, and F. Besenbacher, Phys. Rev. Lett. **76**, 1485 (1996).
[12] G. Binnig, H. Rohrer, Ch. Gerber, and E. Weibel, Appl. Phys. Lett. **40**, 178 (1982).
[13] J. B. Pethica and A. P. Sutton, J. Vac. Sci. Technol. A **6**, 2490 (1988).
[14] C. J. Chen and R. J. Hamers, J. Vac. Sci. Technol. B **9**, 503 (1991).
[15] M. Yoon, H. Mai, and R. F. Willis, Europhys. Lett. **54**, 626 (2001).
[16] W. A. Hofer, Prog. Surf. Sci. **71**, 147 (2003).
[17] G. Binnig, N. Garcia, H. Rohrer, J. M. Soler, and F. Flores, Phys. Rev. B **30**, 4816 (1984).
[18] N. D. Lang, Phys. Rev. B **37**, R10 395 (1988).
[19] L. Olesen, M. Brandbyge, M. R. Sørensen, K. W. Jacobsen, E. Lægsgaard, I. Stensgaard, and F. Besenbacher, Phys. Rev. Lett. **76**, 1485 (1996).
[20] C. J. Chen, in *Scanning Tunneling Microscopy III: Theory of STM and Related Scanning Probe Methods*, edited by R. Wiesendanger and H. J. Güntherodt, Springer Series in Surface Science Vol. 29 (Springer, New York, 1996), p. 141.
[21] V. N. Bogomolov and V. P. Zhuse, Fiz. Tverd. Tela (S.-Peterburg) **10**, 100 (1962) [Sov. Phys. Solid State **5**, 2404 (1963)].
[22] D. A. Bonnell, Prog. Surf. Sci. **57**, 187 (1998).
[23] K. D. Schierbaum, S. Fischer, M. C. Torquemada, J. L. de Segovia, E. Rom, and J. A. Mart-Gago, Surf. Sci. **345**, 261 (1996).
[24] E. H. Rhoderick and R. H. Williams, *Metal-Semiconductor Contacts* (Oxford Science Publications, Clarendon Press, Oxford, 1988).
[25] U. Diebold, J. Lehman, T. Mohmoud, M. Kuhn, G. Leonardelli, W. Hebenstreit, M. Schmid, and P. Varga, Surf. Sci. **41**, 137 (1998).
[26] As the result of the integration times of the amplifiers, small shifts below 0.2 Å occur between the different images.
[27] This change of the tunneling current should carry information of the apparent height but has not been evalutated here.